Experimental and Numerical Investigations on Exergy and Second Law Efficiency of Shell and Helical Coil Heat Exchanger Using Carboxymethyl Cellulose Based Non-Newtonian Nanofluids

Prabhakar Zainith[1] · Niraj Kumar Mishra[1]

Abstract

The main goal of this paper is to study the second law characteristics of carboxymethyl cellulose (CMC)-based non-Newtonian nanofluids with different nanoparticles of aluminum oxide (Al_2O_3), copper oxide (CuO), and titanium oxide (TiO_2) through a helical coil heat exchanger. The present investigation has been carried out for the volume flow rate of non-Newtonian nanofluids ranges from 1 (L·min) to 10 (L·min). In this study, the effect of nanoparticles, nanoparticle volume fraction, and inlet temperature of hot fluid exergy loss, second law efficiency, and heat transfer effectiveness are investigated. It is observed that on increasing the volume flow rate of nanofluids the exergy losses increase for all the nanofluids. Moreover, with the increase in particle volume fraction from 0.01% to 0.04%, the exergy loss reduced by 33%, 30%, and 14% for CuO, Al_2O_3, and TiO_2 nanofluids, respectively, as compared to base fluid, while the exergy loss increases as the inlet temperature of hot fluid increases. Also, the maximum value for second law efficiency is found to be 67% for base fluid, whereas the second law efficiency has been achieved to 71%, 74%, and 77% for TiO_2, Al_2O_3, and CuO non-Newtonian nanofluids, respectively. Therefore, it is concluded from the present study that the use of non-Newtonian nanofluids in helical coil heat exchanger reduces the exergy loss and improves the second law efficiency.

Keywords Exergy loss · Helical coil · Non-Newtonian nanofluids · Second law efficiency

Nomenclature
Re   Reynolds number

✉ Niraj Kumar Mishra
  nkm@nituk.ac.in; nkm.iitg@gmail.com

[1] Department of Mechanical Engineering, National Institute of Technology Uttarakhand, Srinagar (Garhwal) 246174, India

Re_m	Modified Reynolds number
Q	Heat transfer (W)
De	Dean number
De_m	Modified Dean number
q"	Heat flux (W·m^{-2})
Pr	Prandtl number
Pr_m	Modified Prandtl number
E	Exergy loss (W)
S	Entropy (kJ·kg·K^{-1})
d	Coil diameter (m)
D	Diameter, (m)
T	Temperature, (K)
k	Thermal conductivity, (W·m·K^{-1})
Al_2O_3	Aluminum oxide
CuO	Copper oxide
TiO_2	Titanium oxide
η_{II}	Second law efficiency
L	Length
Nu	Nusselt number
h	Heat transfer coefficient (W·m^{-2}·K^{-1})
f_c	Friction factor
n	Flow behavior index
K	Consistency index
u	Velocity (m·s·$^{-1}$)
$\dot{m}$	Mass flow rate (kg·s^{-1})
A_s	Surface area (m^2)
C_p	Specific heat (kJ·kg·K^{-1}
g	Acceleration due to gravity (m·s^{-2})
p	Pitch of coil

Symbols

ρ	Density of fluid, (kg·m^3)
ϕ	Nanoparticle volume concentration
τ	Shear stress
μ	Dynamic viscosity, (Pa·s^{-1})
$\dot{\gamma}$	Shear rate
δ	Curvature ratio, $\left(\frac{d_i}{D_c}\right)$
ψ	Stream exergy
ε	Effectiveness

Subscripts

c	Coil
sh	Shell
bf	Base fluid
nf	Nanofluid

np   Nanoparticle
i   Inlet
o   Outlet
e   Ambient
w   Wall

1 Introduction

Over the past decades, in order to attain enhanced heat transfer for heat exchangers, various techniques have been utilized by the researchers [1]. Among all techniques, researchers focused their interest toward the passive heat transfer techniques. Under the passive heat transfer technique, special surface geometries such as fins, baffles, helical coils, surface coatings, corrugation of tubes, and inserts are frequently utilized in many thermal devices for industrial applications [2–4]. There are many types of traditional heat exchangers reported in the literature. Shell and helical tube heat exchanger gives a superior heat transfer rate compared to traditional heat exchangers. Helical coils have been extensively utilized in various industrial and domestic purposes, for example, air conditioning, refrigeration systems, food processing industries, diary process, and nuclear reactors, due to their concise structure and high heat transfer coefficient [5, 6].

Moreover, the utilization of nanofluids is also a passive technique to enhance the rate of heat transfer. Choi [7] was the first who introduced nanofluids by adding a small concentration of nano-sized particles into a base fluid. Over the last two decades, nanofluids have attracted the attention of the researchers because it has better thermal properties to enhance the rate of heat transfer in various thermal devices [8]. Quantitative evidence of superior heat transfer rate by nanofluids has been reported by various researchers [9–14]. Li et al. [15] experimentally investigated the effects of carbon nanoparticles migration in acetone-based nanofluids for convective heat transfer in a micro-channel heat sink. They reported that heat transfer coefficient and thermo-hydraulic performance were increased by 73% and 69%, respectively. Bahiraei et al. [16] investigated the rate of enhanced heat transfer and hydraulic characteristics with a new ecofriendly graphene-based biological nanofluids for spiral heat exchanger. They concluded that the ratio of heat transfer rate to pressure drop enhances by almost 142% by varying the Reynolds number from 1000 to 3000. Hosseini et al. [17] performed numerical simulations for a shell and tube cooler using carbon nanotube/water-based nanofluids. They illustrated that the thermal performance of the heat exchanger was found superior for all the volume fractions of carbon nanotubes in water.

The first law of thermodynamics gives only the concept of energy balance and is not capable to explain the value of exergy loss during a heat transfer process [18]. At the same time, the second law of thermodynamics gives important information of reduction in quality of energy and its sources. These sources are generally termed as sources of irreversibilities [19]. Exergy is a measure of the deviation of the state for a system with respect to its environment. Moreover, exergy analysis plays a vital role to examine the system losses and hence making the energy system more efficient.

Also, it helps to find out the location, type, and magnitude of wastes and losses in a thermal system [20]. Many researchers used the concept of exergy for the analysis of systems, tools, and various thermal equipment. These devices are generally heat exchangers which transport heat from a hot fluid to a cold fluid. There are several studies reported on the second law of thermodynamics for the qualitative analysis of heat transfer equipment used in different thermal processing units [21, 22]. The common thermal processing units are power plants, geothermal heating, automobiles, and refrigeration and air conditioning plants.

The component-level exergy analysis is also very important in order to identify the critical components of thermal plants and devices under several operating conditions. Therefore, many researchers [23–28] carried out the exergy analysis particularly for shell and tube heat exchangers, instead of the whole thermal unit. Ranjbar et al. [23] conducted the experiments for gas station heaters using twisted tape inserts to study the economics and exergy analysis. They found that the use of inserts enhanced the heat transfer rate by 16% and also improved the exergy efficiency. Esfahani and Languri [24] experimentally studied exergy analysis of a shell and tube heat exchanger using graphene oxide-based nanofluids. In this study, they used two different concentrations 0.01 and 0.1% (by weight) to prepare the nanofluids. They concluded that graphene oxide nanofluid (hot fluid) shows less exergy losses as compared to pure water under the different flow conditions. Jafarzad et al. [25] conducted the experiments to study the energy and exergy performances of a vertical double pipe heat exchanger under the effects of the bubbly flow. The bubbly flow was used to improve the thermal performance. However, they reported that the exergy efficiency of heat exchanger decreases drastically due to the consumption of additional electricity by air compressor to create the bubbly flow.

Wang et al. [26] numerically investigated the exergy and energy analysis for a shell and helically coiled finned tube heat exchangers. They reported that with the increase of heat transfer rate, the exergy loss increases linearly. They also found that the exergy loss is usually equal to 23.4% of the heat transfer rate. Nasirzadehroshenin et al. [27] numerically investigated the exergy analysis of a double pipe heat exchanger using hybrid nanofluid. They concluded that with the increase in mass flow rate and particle volume fraction of nanofluids, the results of exergy efficiency can be improved to a significant amount. Miansari et al. [28] investigated numerically the energy and exergy performance of shell and tube heat exchanger with the effect of adding circular grooves of different sizes. They concluded that the thermal efficiency of the heat exchanger varies from 23 to 49% in various conditions and they also reported that both the flow rate and the inlet temperature have the same effect on the exergy losses.

Based on the above discussion, it is concluded that most of the previous studies related to exergy analysis in helical coil heat exchanger are limited to the Newtonian nature of base fluids. However, due to certain applications of heat transfer fluids in the various industries like polymers industries, food industries, oil industries, pharmaceutical, bio-fluids, tars, paints, and chemical industries, the nature of working fluids are non-Newtonian [29]. Moreover, from previous study by authors [30], it is also concluded that the non-Newtonian nanofluids are found more stable in comparison to Newtonian nanofluids. Therefore, it is required to examine the exergy analysis

of non-Newtonian nanofluids in helical coil heat exchanger. It is also concluded from the literature that there is no study reported related to exergy analysis for the CMC-based non-Newtonian nanofluids in a shell and helical coil heat exchanger. To address this research gap, it is required to analyze the exergetic performance of helical coil heat exchanger based on the second law of thermodynamics to optimize the energy dissipation of helical coil heat exchanger. In this paper, experimental and numerical investigations have been performed for the exergy loss and second law efficiency of a helical coil heat exchanger using CMC/water-based Al_2O_3, CuO, and TiO_2 nanofluids with different volume fractions at different volume flow rate.

2 Experiments

2.1 Sample Preparation

There are two techniques: single-step method and two-step method are generally used to produce stable nanofluids. In the single-step method, vapor deposition, laser ablation, and submerged arc technique are utilized for the preparation of nanofluids [31]. Moreover, in the two-step method prepared nanoparticles are directly mixed with base fluid through the help of some external forces such as ultrasonic vibrations, ball milling, magnetic force agitation, and high shear mixing. The two-step method is widely used for the preparation of nanofluids due to low processing cost and easy to handle.

In the present study, all three types of nanofluids are prepared by two-step method [32]. A flow chart for the preparation of nanofluid is shown in Fig. 1. At first, a small amount of nanoparticle (purchased from Platonic Nanotech private limited, India) is directly added to the distilled water containing 0.4 wt% of CMC. Four different concentrations (0.01, 0.02, 0.03 and 0.04 vol.%) of Al_2O_3, CuO, and TiO_2 nanoparticles are utilized to prepare the nanofluids. The CMC is added to the distilled water to give a non-Newtonian nature to the nanofluid. The mixture of nanoparticles and base fluid is stirred well at 1500 rpm (revolution per minute) for one hour with the
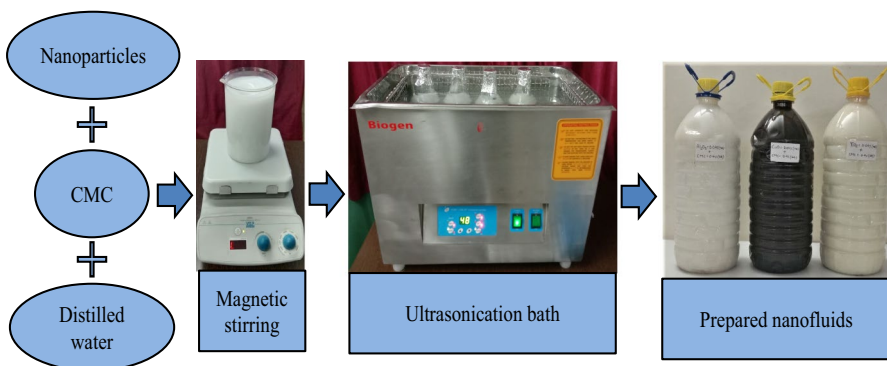

Fig. 1 Preparation of nanofluids

help of a magnetic stirrer (Velp Scientifica) and then placed in the ultrasonic bath (Biogen) with a frequency of 40 kHz for three hours at the temperature of 30^{0}C, this breaks down the agglomeration of particles and also avoids the sedimentation issue.

The stability analysis of nanofluids for the present study was practically observed by conducting visualization stability tests for the different non-Newtonian nanofluids as shown in Fig. 2. It is clear from Fig. 2 that the CuO- and Al_2O_3-based nanofluid show full sedimentation of nanoparticles, while the TiO_2 nanoparticles show some dispersion in the base fluid even after 30 days of preparation. The time taken by the nanoparticles to settle down was found to be 2.5, 3.5, and 4.5 weeks for CuO, Al_2O_3, and TiO_2 nanofluids, respectively. Also, it is documented in previous literature that for a lower volume fraction of nanoparticles (≤ 0.05 vol.%), the stability of nanofluids could be kept for several weeks [33]. Furthermore, as the volume fraction of nanoparticles increases, the stability and required pumping power of nanofluids also get influenced [34]. Therefore, a lower concentration of nanoparticles has been selected for the present study.

2.2 Helical Coils

Helical coils have been reported widely in the literature as it has higher heat transfer rate as compared to conventional tubes [35]. Because of the high heat transfer coefficient and compact structure, helical coils are widely used in different industrial applications such as thermal power plants, refrigeration systems, nuclear industry, heat transfer appliances, food industry, process plants, etc. [36]. Shell and helical tube heat exchangers give a superior heat transfer rate as compared to traditional heat exchangers,
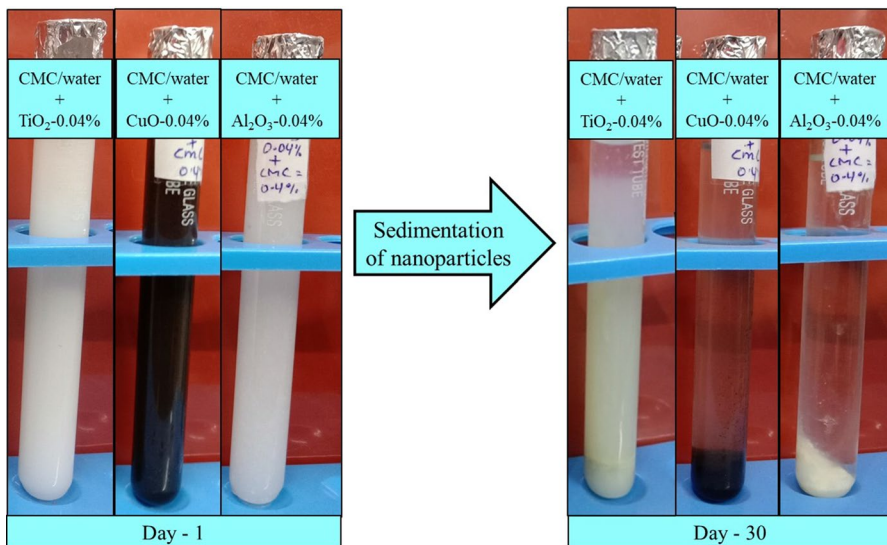

Fig. 2 Sedimentation test of nanofluids

because at the curved section, fluid and nanoparticles try to flow in tangential direction which generates the secondary flow. The secondary flow is induced in the perpendicular direction to the axial flow, which brings the better fluid mixing; thus, the thickness of the thermal boundary layer reduces. In the present study, helical coil of 150 mm diameter is used for the analysis of problem as shown in Fig. 3.

2.3 Thermophysical Properties of Nanofluids

The physical properties such as density, specific heat, and thermal conductivity of 0.4 wt% CMC/water (base fluid) have been considered to be 997.1 (kg·m^{-3}), 4179 (J·kg·K^{-1}), and 0.613 (W·m·K^{-1}), respectively [30, 37, 38]. It is observed from previous experimental investigations that the thermophysical properties of CMC/water (<6 w) are similar to pure water [38]. Therefore, in the present study, the thermophysical properties of 0.4 wt% CMC/water are taken as of pure water. The thermophysical properties of nanoparticles are presented in Table 1 [39, 40]. The required thermophysical properties for the evaluation of exergy loss and second law efficiency are calculated by the Eqs. 1, 2, 5, and 6. These equations have been extensively used in many previous studies to predict the thermophysical properties of nanofluids [27, 29, 36, 39].

The density of nanofluids is evaluated by using the general formula given by Pak and Cho for the mixture [41]:

$$\rho_{nf} = \phi \rho_{np} + (1 - \phi)\rho_{bf} \tag{1}$$

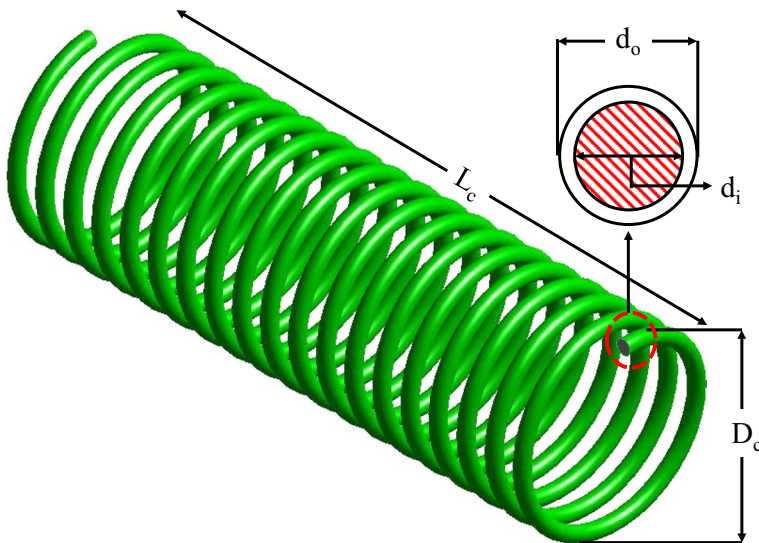The specific heat of the nanofluids given by Xuan and Roetzel can be calculated as follows[42]:

Fig. 3 Dimensions of helical coil used in the present study

Table 1 Thermophysical properties of nanoparticles

Properties	Al_2O_3	CuO	TiO_2
Average particle size	30–40 nm	40–60 nm	30–50 nm
Specific surface area	60–80 $m^2 \cdot g^{-1}$	30–50 $m^2 \cdot g^{-1}$	200–230 $m^2 \cdot g^{-1}$
True density	3.97 $g \cdot cm^{-3}$	6.4 $g \cdot cm^{-3}$	4.23 $g \cdot cm^{-3}$
Specific heat	765 $J \cdot Kg \cdot K^{-1}$	530 $J \cdot Kg \cdot K^{-1}$	680 $J \cdot Kg \cdot K^{-1}$
Thermal conductivity	38–43 $W \cdot m \cdot K^{-1}$	30–33 $W \cdot m \cdot K^{-1}$	8–12 $W \cdot m \cdot K^{-1}$

$$C_{P_{nf}} = \frac{\phi \rho_{np} C_{P_{np}} + (1-\phi)\rho_{bf} C_{P_{bf}}}{\rho_{nf}} \tag{2}$$

As mentioned in the prior literature that the addition of 0.4 wt% CMC to pure water changes the nature of the base fluid from Newtonian to non-Newtonian [43, 44], in the present study, the values of consistency index (K) and flow behavior index (n) for the mixture of 0.4 wt% CMC and water are considered 0.376 (Pa·s^n) and 0.58, respectively [45]. The power law model for viscous fluids is described as follows:

$$\tau = K\dot{\gamma}^n \tag{3}$$

where τ and $\dot{\gamma}$ are the shear stress and shear rate, respectively. The apparent viscosity (μ_a) of non-Newtonian fluids is expressed as follows:

$$\mu_a = K\dot{\gamma}^{n-1} \tag{4}$$

Einstein equation for concentrations less than 5 vol.% can be utilized to calculate the viscosity of nanofluids as follows[46]:

$$\mu_{nf} = \mu_{bf}(1 + 2.5\phi) \tag{5}$$

The Wasp model [47] is used to calculate the thermal conductivity of nanofluids:

$$\frac{k_{nf}}{k_{bf}} = \frac{k_{np} + 2k_{bf} - 2\phi(k_{bf} - k_{np})}{k_{np} + 2k_{bf} + \phi(k_{bf} - k_{np})} \tag{6}$$

2.4 Experimental Set-Up and Procedure

The schematic diagram of the experimental setup is shown in Fig. 4. It consists of a test section, storage units of hot and cold fluids, and circulation arrangements for hot and cold fluids. The test section is a counter flow single-pass horizontal shell and helical coil heat exchanger. The helical coil is made up of copper, while the material of shell for heat exchanger is mild steel. The outer shell of the test section is insulated by a glass wool of 20 mm thickness and also covered by aluminum foil at the top to avoid heat losses to the surroundings. The physical dimensions of the
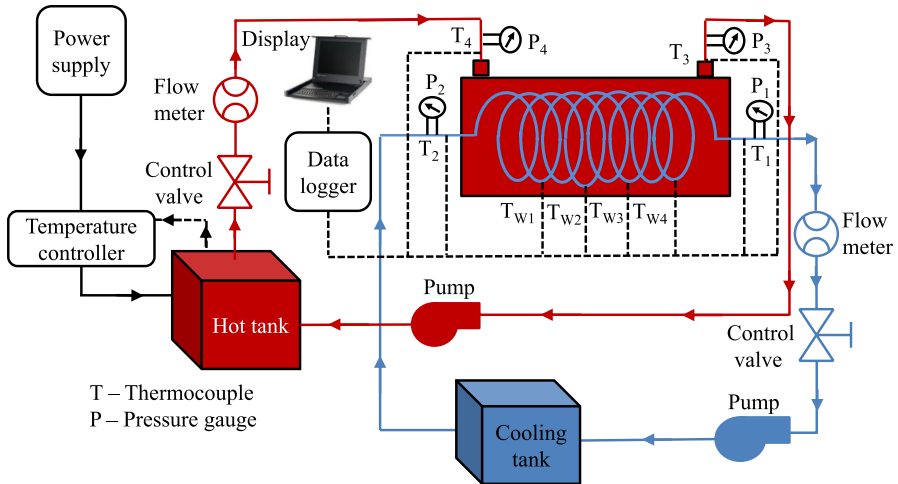
Fig. 4 Schematic diagram of experimental set-up

shell and helical coil heat exchanger are presented in Table 2. An electric heater of 1500 (W) is used to heat the water of hot tank and the temperature is maintained constant by using a temperature controller. Besides, a refrigerated cooling tank is used to cool the nanofluid. Each circulation arrangement consists of a flow meter (Broil Sensotek Industries, India) and control valve, used to measure and control the volume flow rate, respectively. The range of flow meter varies from 0.8 (L·min^{-1}) to 83.33 (L·min^{-1}) with an accuracy of $\pm 0.75\%$. The total 9 number of K-type thermocouples (Tempsens Instruments Pvt. Ltd. India) are used to measure the temperature at different sections of the heat exchanger. The range of thermocouples are -200 °C to 1260 °C with an accuracy of $\pm 0.75\%$. Pressure gauge (H. Guru Industries, India) ranges from 0 to 5 bar with an accuracy of $\pm 1\%$ are fitted at the ends of the test sections to measure the pressure difference. The pumps are used to circulate the fluids throughout the circulation arrangements of heat exchanger.

Table 2 Dimensions of Heat Exchanger		
Length of the shell (L_{sh}), mm		540
Helical Coil length (L_c), mm		500
Coil diameter (D_c), mm		150
Pitch of coil (p_c), mm		09
Outer coil tube diameter (d_o), mm		12.72
Inner coil tube diameter (d_i), mm		10.80
Curvature ratio $\left(\frac{d_i}{D_c}\right)$		0.072
Number of turns (N)		19
Outer diameter of shell ($D_{sh,o}$), mm		216
Inner diameter of shell ($D_{sh,i}$), mm		210

A general view of the experimental setup is shown in Fig. 5. The nanofluid is pumped into the helical coil supplied through a cooling tank at various volume flow rate ranges from 1 (L·min^{-1}) to 10 (L·min^{-1}). The present study is investigated under laminar flow region for non-Newtonian nanofluids, the value of modified Reynolds number for the given volume flow rate ranges from 37 to 980. Also, the Dean number ranges from 10 to 270 for the same volume flow rate. The hot fluid (water) is supplied through a hot tank equipped with an electric heater. The hot fluid has been allowed to flow through shell side of heat exchanger and volume flow rate of hot fluid is kept constant at 10 (L·min^{-1}). Initially, both the fluids are allowed to flow till the steady state was reached. Once the steady state is reached, all the measurable parameters were noted down. Now the process was repeated for three different nanoparticles (Al_2O_3, CuO and TiO_2) and four different nanoparticle concentrations (0.01%, 0.02%, 0.03% and 0.04%). All the experiments have been repeated three times for better accuracy of the results.

2.5 Data Analysis

2.5.1 Calculation of Nusselt Number and Friction Factor

To calculate the Nusselt number and friction factor for pure water, following formulations have been used:

Reynolds number:
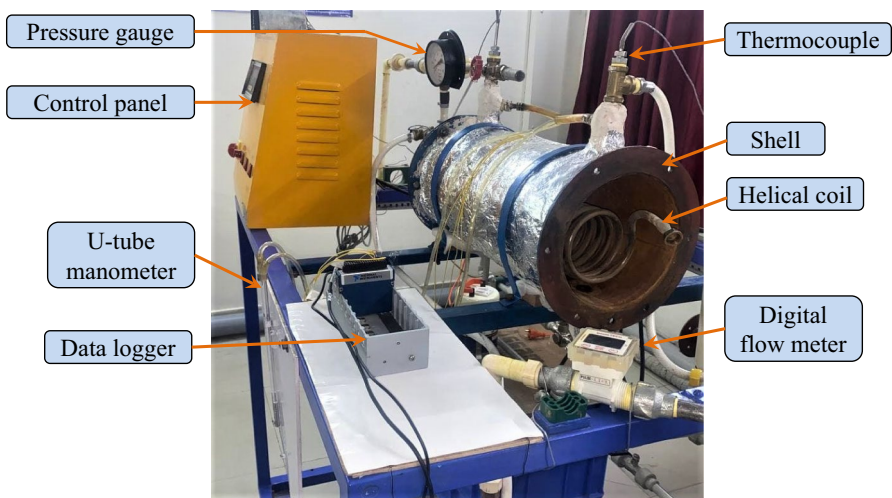
$$Re = \frac{\rho u_m d_i}{\mu} \tag{7}$$

Dean number:

Fig. 5 Pictorial view of test section

$$D_e = \frac{R_e}{\left(\frac{d_i}{D_C}\right)^{0.5}} \tag{8}$$

Prandtl number:

$$Pr = \frac{C_p \mu}{k} \tag{9}$$

The present study has been carried out for heat transfer analysis of non-Newtonian nanofluids. Therefore, all mathematical calculations are carried out considering power law model, for power law model parameters such as consistency index and flow behavior index are utilized. The following modified dimensionless numbers are used to predict the Nusselt number:

Reynolds number was used by Metzner and Reed for non-Newtonian fluids [48]:

$$Re_m = \frac{d_i^n u^{2-n} \rho}{K \left(\frac{1+3n}{4n}\right)^n 8^{n-1}} \tag{10}$$

Modified Dean number and modified Prandtl number were used by Pimenta and Campos [45]:

$$De_m = Re_m \left(\frac{d_i}{D_c}\right)^{0.5} \tag{11}$$

Modified Prandtl number:

$$Pr_m = \frac{C_P}{k_f} K \left(\frac{u}{d_i}\right)^{n-1} \left(\frac{3n+1}{4n}\right)^n 8^{n-1} \tag{12}$$

Coil side heat transfer (W):

$$\dot{Q}_C = \dot{m} C_p \left(T_{C,o} - T_{C,i}\right) \tag{13}$$

Heat flux (W·m^{-2}):

$$q'' = \frac{\dot{Q}_C}{A_{S,c}} \tag{14}$$

The average heat transfer coefficient and Nusselt number are calculated as follows:

$$h_{c,avg} = \frac{q''}{T_{W,avg} - T_{C.avg}} \tag{15}$$

Nusselt number:

$$Nu = \frac{h_{c,avg}d_i}{k} \tag{16}$$

The friction factor for helical coils is calculated by the following equation [49]:

$$f_c = \frac{\Delta P d_i^5 \rho \pi^2}{32 L_{coil}\dot{m}^2} \tag{17}$$

2.5.2 Exergy Loss and Second Law Efficiency Calculations

Exergy loss represents the rate of irreversibility for a thermodynamic process. Consequently, it is a crucial factor for measuring the quality of thermal devices. Every thermodynamic system has some losses in terms of heat and pressure losses. The exergy analysis is the best way to find these losses and optimize the energy losses of the system. Hence, the exergy characteristics for the given heat exchanger can be calculated as follows [50].

For a steady-state control volume process, the exergy balance equation can be written as follows:

$$\sum E_{in} = \sum E_{out} - \sum E_{product} \tag{18}$$

The total exergy loss (E) of a steady-state open system can be calculated as follows:

$$E = E_h + E_c \tag{19}$$

where E_h and E_c represent the exergy change of hot and cold fluid. E_h and E_c can be evaluated by the following two equations:

$$E_h = T_e\left[m_h\left(S_{h,out} - S_{h,in}\right)\right] \text{or}, E_h = T_e\left[C_h\ln\left(\frac{T_{h,out}}{T_{h,in}}\right)\right] \tag{20}$$

$$E_c = T_e\left[m_c\left(S_{c,out} - S_{c,in}\right)\right] \text{or}, E_c = T_e\left[C_c\ln\left(\frac{T_{c,out}}{T_{c,in}}\right)\right] \tag{21}$$

where C_h and C_c are the heat capacity (kW·K^{-1}) of hot and cold fluid, respectively.

From Eqs. 20 and 21, the exergy loss according to Eq. 19 can be calculated as follows:

$$E = T_e\left[C_h\ln\left(\frac{T_{h,out}}{T_{h,in}}\right) + C_c\ln\left(\frac{T_{c,out}}{T_{c,in}}\right)\right] \tag{22}$$

The second law efficiency for open system is defined as the ratio of exergy recovered to exergy expanded [51]. For a shell and helical coil heat exchanger, exergy recovered is the sum of rise in exergies of helical coil (cold fluid), while the exergy expanded is the decrease in exergies of shell fluid (hot fluid):

$$\eta_{II} = \frac{Exergy\ recovered}{Exergy\ expanded} = \frac{\dot{m}_{nf}\left(\psi_{nf,out} - \psi_{nf,in}\right)}{\dot{m}_{hot}\left(\psi_{hot,in} - \psi_{hot,out}\right)} \tag{23}$$

In the above equation, the term ψ represents the stream exergy and calculated as follows[52]:

$$\psi = \left(h - h_e\right) - T_e\left(s - s_e\right) \tag{24}$$

where s and h indicate the entropy and enthalpy, respectively.

The heat transfer effectiveness (ε) can be calculated as follows:

$$\varepsilon = \frac{\dot{Q}}{\dot{Q}_{max}} = \frac{Actual\ heat\ transfer\ rate}{Maximum\ possible\ heat\ transfer\ rate} \tag{25}$$

where actual and maximum possible heat transfer rate can be expressed as follows:

$$\dot{Q} = C_c\left(T_{c,out} - T_{c,in}\right) = C_h\left(T_{h,in} - T_{h,out}\right) \tag{26}$$

$$\dot{Q}_{max} = C_{min}\left(T_{h,in} - T_{c,in}\right) \tag{27}$$

Ideally, for a shell- and tube-type heat exchanger, the heat transfer rate of the cold side and hot side should be equal. But in a practical situation, even after proper insulation of the heat exchanger, some amount of heat is always dissipated to the environment. In the present study, a heat loss analysis has been carried out to calculate the amount of dissipated heat to the surroundings. From the heat loss analysis, it is found that the difference between the heat transfer rate of the cold side and the hot side is less than 3% for all cases. The similar range of heat loss has been reported in a previous study for a double pipe heat exchanger [25]. Thus, it is reliable to use same values of heat transfer rates for hot and cold fluids to evaluate effectiveness of heat exchanger.

2.6 Uncertainty Analysis

Various fixed and random errors in experimental measurement cause inaccuracy. Therefore, the analysis of uncertainty is very important to determine the acceptable range of variations in experimental results from true values. The following equation has been used to evaluate all the errors [53]:

$$maxU_P = \pm\left[\left(\frac{X_1}{P}\frac{\partial P}{\partial X_1}U_1\right)^2 + \left(\frac{X_2}{P}\frac{\partial P}{\partial X_2}U_2\right)^2 + \ldots\ldots\ldots\ldots\ldots\left(\frac{X_i}{P}\frac{\partial P}{\partial X_i}U_i\right)^2\right]^{0.5} \tag{28}$$

The uncertainty in an experimental study is defined by its measurable parameters, for example, temperature, volume flow rate, specific heat, and thermal conductivity. The total uncertainty by these errors has been estimated by the following equation [54]:

$$MaxU_E = \pm \left[\left(U_{\dot{m}} \right)^2 + \left(U_{Cp} \right)^2 + \left(U_T \right)^2 \right]^{0.5} \tag{29}$$

Digital flow meters are utilized to measure the volume flow rate with an uncertainty of 0.85%. The uncertainty in temperature is found to be 0.75%, which is measured by K-type thermocouples. In this study, Xuan and Roetzel model and Wasp model (Eqs. 2 and 6) are used to predict the specific heat and thermal conductivity of non-Newtonian nanofluids, respectively. It is presumed that uncertainty for specific heat and thermal conductivity is 2.0% and 4%, respectively [55]. The maximum uncertainty in the Nusselt number is found to be $\pm 4.6\%$, while for exergy loss and second law efficiency it is $\pm 2.3\%$.

2.7 Numerical Simulations

Besides the experimental analysis, the study is also focused on numerical findings. The main goal of the numerical study is to validate the simulated values with experimental results and to find its percentage deviation. In this section, the numerical simulations of exergy loss and second law efficiency for a shell and helical coil heat exchanger using CMC-based non-Newtonian nanofluids are presented.

Initially, a three-dimensional geometrical model of the present study is created in the ANSYS design modeler as shown in Fig. 6a. The same dimensional parameters are modeled as used in the experimental set-up. The next step was the meshing for created model and for the same ANSYS mesh model was utilized for the mesh generation. The meshing of shell and helical coil is presented in Fig. 6d, c, respectively. The FLUENT 19 is used for CFD code to solve the numerical problem. A pressure-based solution algorithm has been used as a solver. The governing equations are solved iteratively, as demonstrated in the flow chart diagram shown in Fig. 7. Finite volume technique is utilized with second-order accuracy under laminar flow condition. SIMPLEC algorithm has been selected, to handle the velocity. The convergence criterion chosen for momentum and energy equation is 1.0E–06, while for the Continuity equation it is 1.0E–03. Numerical simulations of nanofluids are conducted using single phase homogenous model. In this model, the main assumption is that the base fluid and the nanoparticle are in thermal equilibrium with zero relative velocity. In order to simplify the present problem, since the thickness of the helical tube is very small (0.96 mm), the conductive heat transfer of the helical tube has not been considered. In the present study, power law model is utilized instead of constant viscosity model, as the present study emphasizes on non-Newtonian nanofluids. The non-Newtonian fluids are treated as complex fluids. Therefore, the following assumptions were made for the analysis of numerical problem:

(i) 3-D Fluid flow in the shell and helical coil heat exchanger.
(ii) Steady-state flow condition.
(iii) No heat transfer takes place from the outer wall of the shell.
(iv) Incompressible and laminar fluid flow condition.
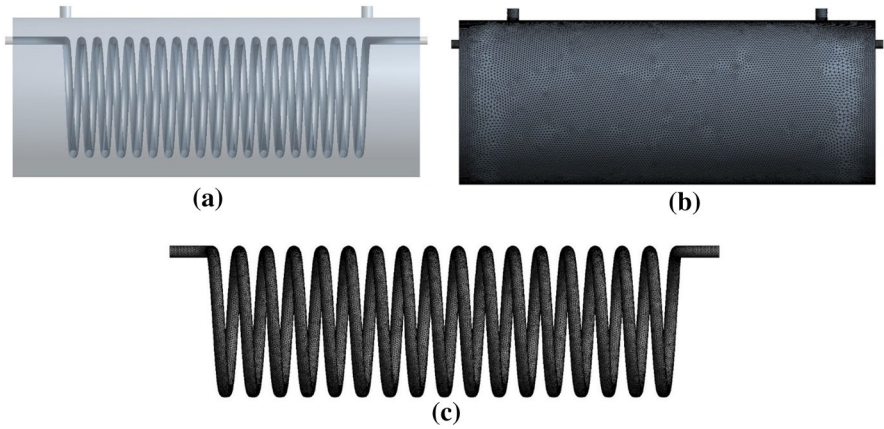(v) Single phase approach for fluid flow with the non-Newtonian power law model.

Fig. 6 (a) 3-D model of shell and helical coil, (b) meshing of shell and **c** meshing of helical coil
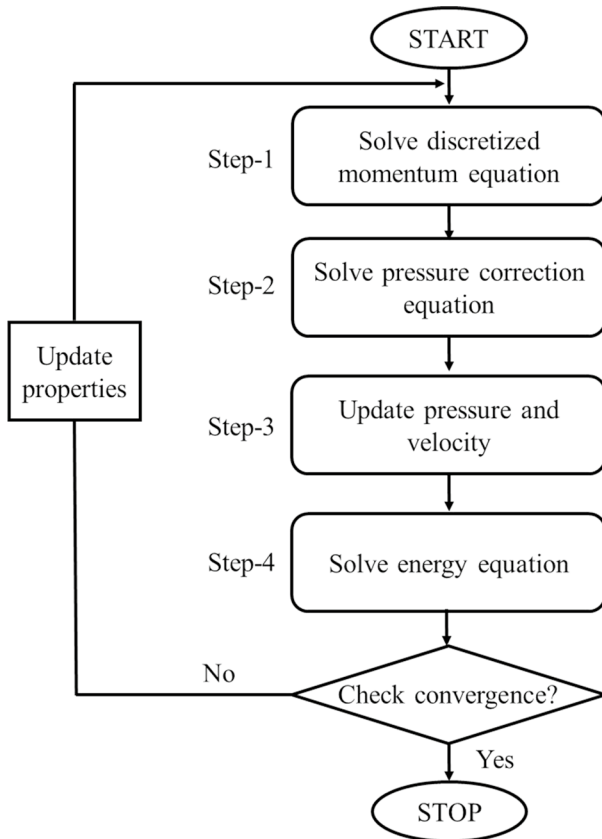

Fig. 7 Flow chart for pressure-based solution algorithm

(vi)   Velocity change between nanoparticles and the base fluid is negligible.

(vii)   No Radiation takes place.

(viii)   No internal heat generation.

The basic governing equations which are utilized for the fluid flow and heat transfer analysis are as follows: continuity equation, momentum equation, and energy equation are given below.

Continuity equation:

$$\nabla\left(\rho_f u_f\right) = 0 \tag{30}$$

Momentum equation:

$$\nabla\left(\rho_f u_f u_f\right) = -\nabla P + \rho g + \left(\mu_f . \nabla u_f\right) \tag{31}$$

Energy equation:

$$\rho_f C_{p,f}\left(u_f \nabla T\right) = k_f\left(\nabla^2 T\right) \tag{32}$$

2.8 Boundary Conditions

In this study, single phase approach has been followed with power law model as the nanofluid is non-Newtonian in nature. At the helical coil inlet, the volume flow rate varies from 1 (L·min^{-1}) to 10 (L·min^{-1}). The inlet temperature of nanofluid (helical coil) has been taken as 20 °C (T$_i$). While the shell side fluid is water and allow to flow with three different inlet temperatures of 35 °C, 45 °C, and 55 °C, and volume flow rate is kept constant at 10 (L·min^{-1}). The outer wall of heat exchanger is considered to be adiabatic. For the present study, the simplified boundary conditions comprise of three parts which are velocity inlet, pressure outlet, and wall. At the inlet, velocity inlet condition is used in the normal direction to the boundary with specified inlet temperature. At the outlet, pressure outlet condition is used, i.e., the value of outlet pressure has been considered as zero (gauge pressure). The fluid velocity on the wall surfaces is zero, which represents the no-slip condition. The detailed boundary conditions are presented in Table 3.

2.9 Grid-Independent Test

The unstructured tetrahedral mesh model is generated in ANSYS 19 and the same has been demonstrated in Fig. 6. A Grid-independent test has been performed to find the most appropriate mesh size for accurate results and to reduce the required simulating time for the higher order of mesh size. The test is performed under laminar flow region for pure water at a Reynolds number of 3078 of coil side of heat exchanger. For pure water, at a volume flow rate of 2 (L·min^{-1}), the corresponding value of Reynolds number is 3078, which falls under the laminar flow region. The critical Reynolds number

Table 3 Boundary conditions	Boundary conditions	Details
	Coil inlet	Inlet velocity value is known and the velocity vectors are normal to inlet surface, $T_i = 20$ °C
	Coil outlet	Pressure outlet
	All walls	No slip condition
	Shell inlet	$T_{Si} = 35$ °C, 45 °C and 55 °C
	Shell outlet	Pressure outlet
	Viscosity	Power law model for non-Newtonian flows

is calculated for pure water using correlation (Eq. 33) developed by Mishra and Gupta [56] for helical coils and the value for critical Reynolds number is found 8616. The inlet temperature of coil side and shell side are kept 293 (K) and 328 (K), respectively. The coil side Nusselt number was compared at 5 different mesh sizes, as shown in Fig. 8. Among all the grid sizes only three grid sizes (5.5×10^6, 6.1×10^6 and 6.4×10^6) give the near around the same values. Consequently, the grid size of 5.5×10^6 elements is utilized for the present study.

$$Re_{cr} = 20000 \left[\frac{d_i}{D_c \left[1 + \left(\frac{p_c}{\pi D_c}\right)^2\right]} \right]^{0.32} \left\{ 0.004 < \frac{d_i}{D_c} < 0.1 \right\} \tag{33}$$
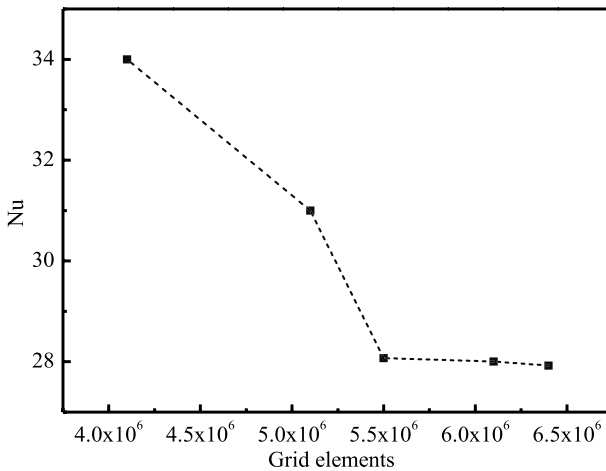

Fig. 8 Grid-independent test for coil side Nusselt number at Re = 3078 with pure water

3 Results and Discussion

3.1 Validation with Pure Water

To verify system ability and procedure reliability, experiments are performed with pure water before the analysis for 2nd law characteristics of the present problem. The experimental Nusselt number of the present study is validated with numerical results as shown in Fig. 9a. Also, the results are compared with those obtained from the correlations given by Dravid et al. [57] and Pimenta and Campos [45] for water. The correlation was defined as follows:

Dravid et al. [57]:

$$Nu = \left(0.76 + 0.65 \times De^{0.5}\right)Pr^{0.175} \left\{ \begin{array}{c} 50 \leq De \leq 2000 \\ 5 \leq Pr \leq 175 \end{array} \right\} \tag{34}$$

Pimenta and Campos [45]:

$$Nu = (0.5De^{0.481} - 0.465)Pr^{0.367} \tag{35}$$

The maximum variation in numerical studies with the experimental results is found 13.9%. While, with the correlations the experimental values are found in good agreement, the maximum deviation with correlations described by Eqs. 34 and 35 are found 4.8% and 13.8%, respectively.

Moreover, for the authenticity of results, the experimental results are also validated with friction factor as shown Fig. 9b. The validation has been done for 0.4% CMC with water (base fluid) with numerical results and developed correlations. The correlation for friction factor given by Mashelkar and Devrajan [58] is presented in Eq. 36; for the same, the validation has been carried and the maximum variation is found to be 10.7%, while the numerical results are maximum deviated by 18.33%.
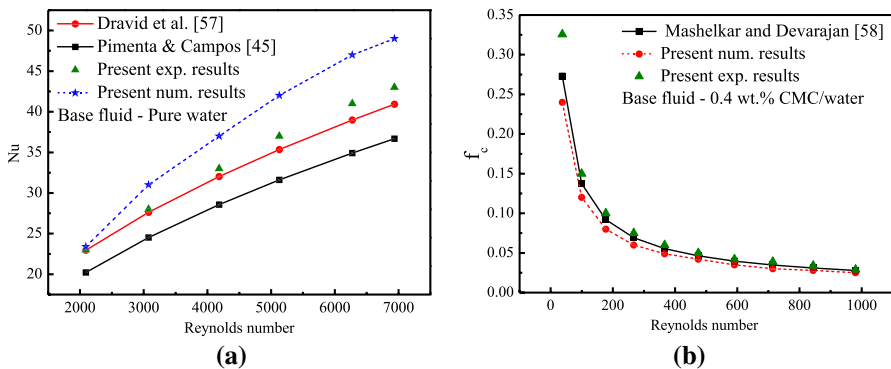

Fig. 9 Validation of Nusselt number (a) and friction factor (b) with different correlations and numerical results

$$f_c = \left(\left(9.069 - 9.438n + 4.37n^2 \right) \left(\frac{d_i}{D_c} \right)^{0.5} De_m^{-0.768+0.122n} \right) \left\{ \begin{array}{c} 0 \leq De_m \leq 400 \\ 0.01 \leq \frac{d_i}{D_c} \leq 400 \\ 0.358 \leq n \leq 1 \end{array} \right\}$$

(36)

where De_m is the modified Dean number.

3.2 Exergy Loss

In this section, exergy loss of three different types of CMC-based non-Newtonian nanofluids with different particle concentrations for the helical coil heat exchanger is presented. The exergy loss for three different types of nanoparticles Al_2O_3, CuO, and TiO_2 with four different particles concentrations (0.01 to 0.04 vol.%) at different volume flow rates of nanofluids ranges from 1 (L·min^{-1}) to 10 (L·min^{-1}), as shown in Fig. 10. It is clear from Fig. 10 that on increasing volume flow rate of nanofluids the total exergy loss increases. The above statement can be clarified by Eq. 22, the term heat capacity (C) in the equation is the product of mass flow rate and specific heat. Thus, as the volume flow of nanofluid increases from 1 (L·min^{-1}) to 10 (L·min^{-1}), the magnitude of heat capacity for nanofluids increases. The volume flow rate of hot fluid is kept constant at 10 (L·min^{-1}), thus the heat capacity of hot fluid is constant throughout the process. As the flow rate increases in helical coil, the turbulence level of secondary flow increases. Thus, the irreversibility of the system increases, which results in increase of the exergy loss.

Figure 10 also demonstrates the exergy loss with the variation in particle concentrations. As is obvious, the exergy loss reduces by employing the nanoparticles to base fluid. This reveals that as the particle concentration increases, considerable reduction occurs in the loss of available energy. On increasing particle concentration from 0.01% to 0.04 vol.%, the total exergy loss reduced by 14%, 30%, and 33% for TiO_2, Al_2O_3, and CuO nanofluids, respectively, as compared to the base fluid. It is also found that on increasing particle volume concentration, the temperature gradient of nanofluids decreases resulting in decrease of the thermal entropy generation. At the same time, the temperature gradient of hot fluid increases and enhances the generation of thermal entropy. But the reduction rate of thermal entropy generation of nanofluids is much higher than the increase in generation of thermal entropy of hot fluid. Consequently, the overall decrement is noted in exergy loss of shell and helical coil heat exchanger as particle concentrations increase, this indicates the domination of reduction in the exergy loss due to the addition of nanoparticles over the increment in the exergy loss of hot fluid.

Moreover, a numerical study has been performed to understand the results in a better way. The numerical study has been carried out under similar operating conditions as performed in the experimental study. Figure 11 shows a comparison between experimental and numerical results for exergy losses. It is clear from Fig. 11 that the maximum deviations in numerical results are 15.5%, 15%, and 16% for Al_2O_3, CuO, and TiO_2 nanofluids, respectively. The losses in experimental values are higher because most of the unwanted losses are not considered in the experimental process, while the
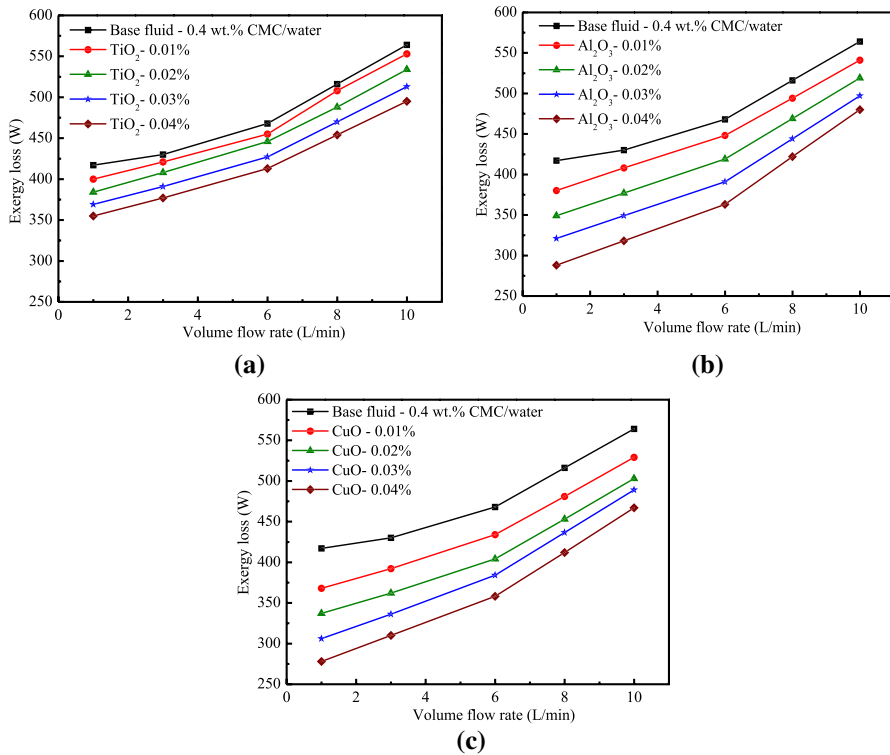
Fig. 10 Total exergy loss of hot and cold fluid (nanofluid) with different volume flow rates of nanofluids at different particle concentration ranges from 0.01 vol.% to 0.04 vol.% for (a) TiO_2, (b) Al_2O_3, and (c) CuO nanofluids

numerical results are assumption-based. Thus, the losses in numerical studies are quite low as compared to experimental studies.

As stated before, the exergy losses reduced by 33%, 30%, and 14% for CuO, Al_2O_3, and TiO_2 nanofluids, respectively. This is attributed due to the temperature gradient across the test section. The temperature contours have been presented in Fig. 12. The temperature contours have been shown for the different nanofluids at a particular volume fraction of 0.04% and volume flow rate of 1 (L·min^{-1}). It is clear from the temperature contours that the temperature gradient of shell side fluid for TiO_2 nanofluids is quite low than the CuO and Al_2O_3 nanofluids. While the temperature gradient of coil side nanofluids is higher for TiO_2-based nanofluids compared to CuO and Al_2O_3 nanofluids. These temperature gradients are varied, as the particle and particle concentration are changed, which is the main reason for the changes in exergy loss of hot and cold fluid.
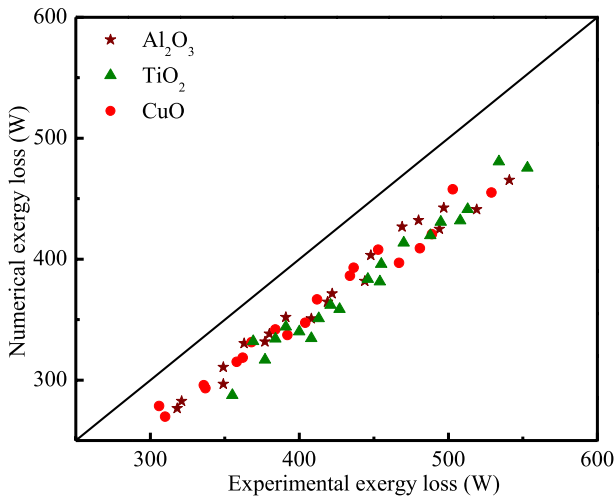
Fig. 11 Variation in experimental and numerical results for exergy loss

3.3 Second Law Efficiency

In this section, second law efficiency is discussed with different volume flow rate and particle concentrations. The variation in volume flow rate and particle concentration of Al_2O_3, CuO, and TiO_2 nanofluids is shown in Fig. 13. From Fig. 13, it is clear that on increasing volume flow rate of nanofluids and particle concentration the exergetic efficiency increases. The second law efficiency of base fluid is found to increase from 58 to 67% on varying the volume flow rate from 1 to 10 $(L \cdot min^{-1})$. It is observed that adding nanoparticles to the base fluid improves the second law efficiency. The maximum second law efficiency is found to be 77%, 74%, and 71% for CuO, Al_2O_3, and TiO_2 nanofluids, respectively, at a particle volume fraction of 0.04% and volume flow rate of 10 $(L \cdot min^{-1})$.

The main reason for the enhancement in exergetic efficiency is the drastic changes in the heat transfer process. These changes occur due to enhancement of thermal conductivities of nanofluids by adding nanoparticles to the base fluid. Higher rate of heat transfer leads to reduce the destruction of available work or reduction in exergy loss, consequently the second law efficiency increases. Another reason of the improved thermal conductivity is the random motion (Brownian motion) of nano particles in the base fluid. The effect of Brownian motion increases as volume flow rate of nanofluid increases. Moreover, secondary flow of nanofluids generated due to the helical coil which results in higher rate of heat transfer. Secondary flow increases the random motion of nano particles, which may break the thermal boundary layer. Above factors collectively cause more heat transfer, this leads to reduce the exergy loss.

Figure 14 shows the deviation in numerical results with experimental values for second law efficiency. It can be seen from Fig. 14, that numerical results are in
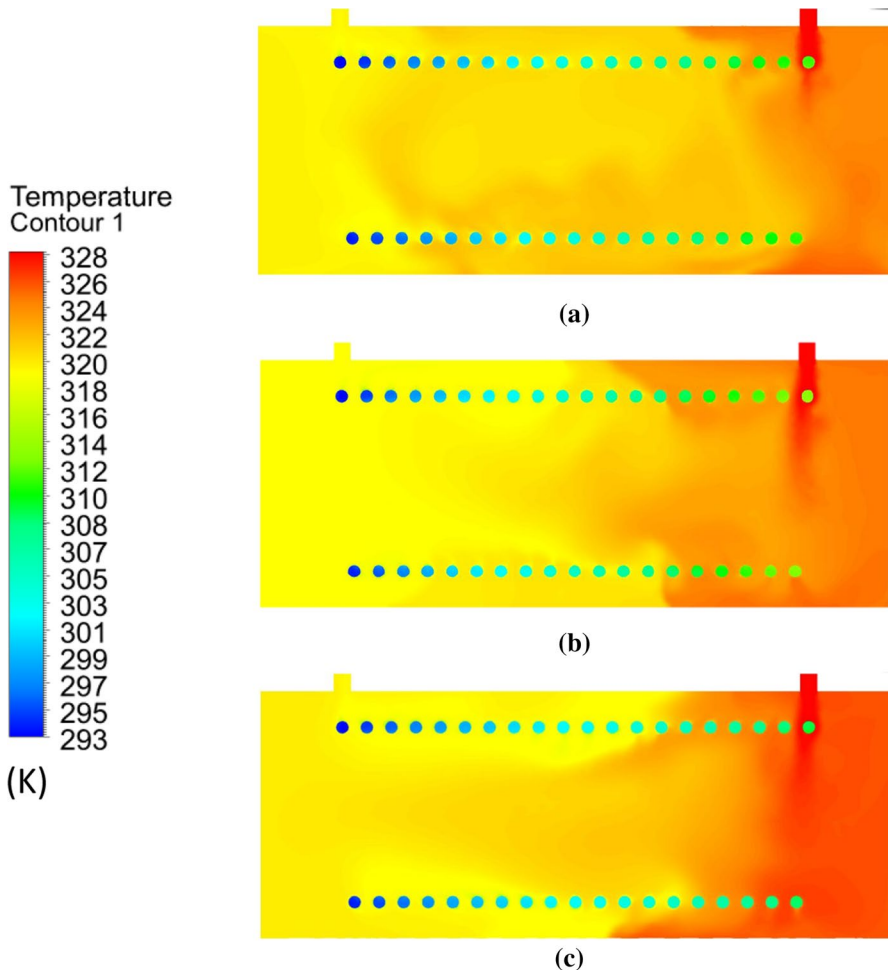
Fig. 12 Contours of temperature at a volume flow rate of 1 (L·min^{-1}) (a) TiO$_2$ nanofluids, (b) CuO nanofluids, and (c) Al$_2$O$_3$ nanofluids

good agreement as compare to experimental results with a maximum deviation of 13%, 14.5% and 17% for Al$_2$O$_3$, CuO and TiO$_2$ nanofluids respectively.

3.4 Change in Exergy Loss with Inlet Temperature of Hot Fluid

Figure 15 shows the variation in exergy loss of TiO$_2$, Al$_2$O$_3$ and CuO nanofluids with three different inlet temperatures (35 °C, 45 °C and 55 °C) of hot fluid at a volume flow rate of 6 (L·min^{-1}) for nanofluids. While the volume flow rate of shell side (hot fluid) is kept constant at 10 (L·min^{-1}). It is clear from the Fig. 15 that on increasing the inlet temperature of hot fluid the exergy losses increase. This is attributed due to temperature gradient between hot and cold fluid. If the temperature
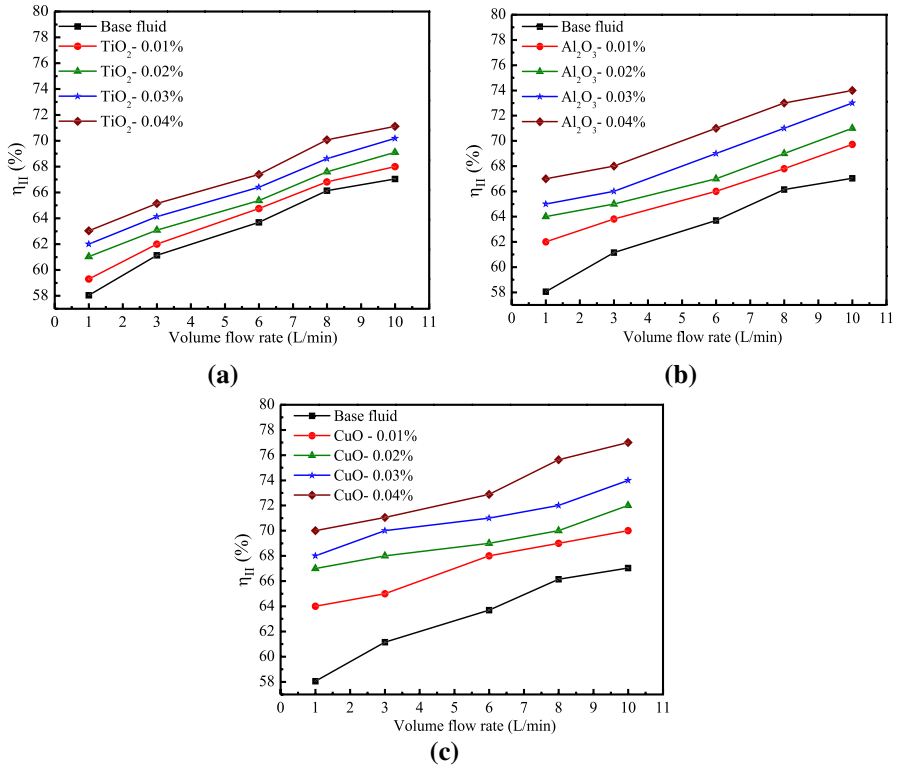
Fig. 13 Second law efficiency at different particle concentrations and volume flow rate for (a) TiO_2 nano-fluids, (b) Al_2O_3 nanofluids, and (c) CuO nanofluids
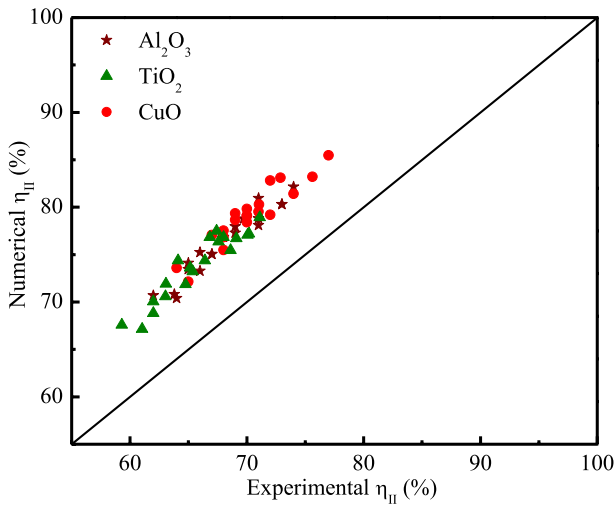

Fig. 14 Variation in experimental and numerical results for second law efficiency
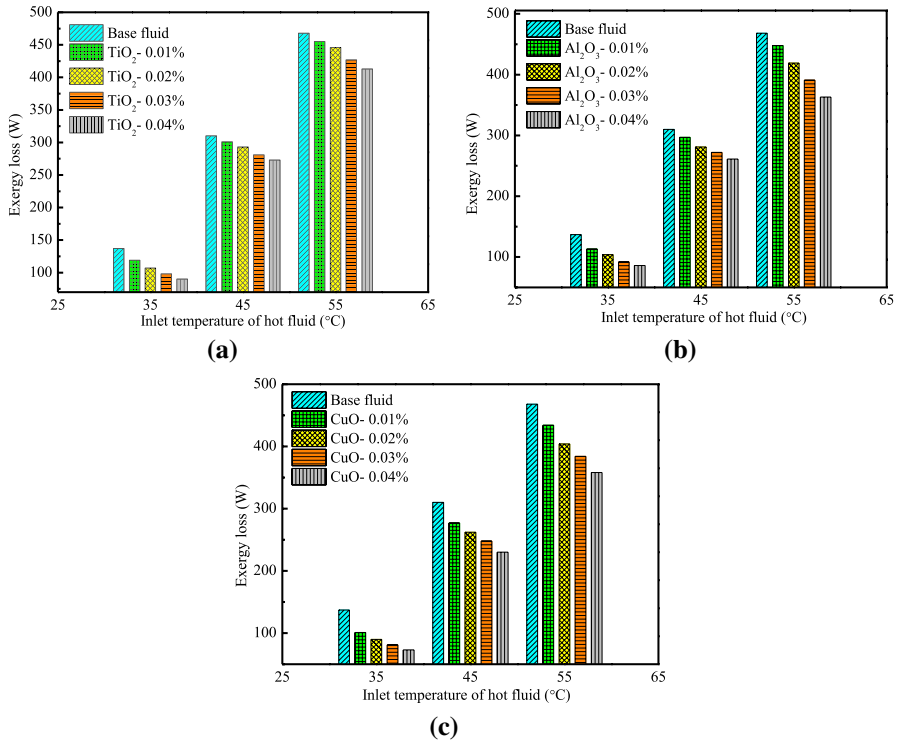
Fig. 15 Variation in exergy loss with the change in hot fluid inlet temperature for (a) TiO_2 nanofluids, (b) Al_2O_3 nanofluids and (c) CuO nanofluids

difference is increasing between the working fluids of heat exchanger, the exergy losses also increasing. Moreover, at lower intel temperatures (35 °C and 45 °C) of hot fluid, the temperature gradients of hot and cold fluid follow similar trends as discussed in Sect. 4.2. The maximum exergy loss for base fluid at a volume flow rate of 6 (L·min^{-1}) is found 310 (W) and 137 (W) at hot fluid inlet temperatures of 45 °C and 35 °C respectively, while at 55 °C the exergy loss is 468 (W). It is due to the entropy generation is much lower at lower inlet temperatures as compared to higher inlet temperatures of hot fluid. From the Fig. 15a–c it is obvious, that the exergy loss for all the nanofluids decreases on increasing the particle concentration and also with the inlet temperatures. Thus, according to the second law analysis of the present investigation, the utilization of non-Newtonian nanofluids with combination of helical coils is recommended as this type of combinations can reduce the destruction of available work and enhance the thermal performance of heat exchangers.

3.5 Effectiveness of Heat Exchanger

Effectiveness is defined as the ratio of actual heat transfer to the maximum possible heat transfer. The main purpose of effectiveness is to predict the thermal

performance of any heat exchanger. The thermal performance of a shell and tube heat exchanger under certain specific conditions is generally expressed in terms of effectiveness, which is a function of the change in temperature of the hot and cold fluids. The effects of volume flow rate and particle concentration of nanofluids on effectiveness have been discussed in this section. Figure 16 shows the variation of effectiveness with volume flow rate for different nanofluids (TiO$_2$, Al$_2$O$_3$ and CuO) at different particle concentrations. It is clear from Fig. 16 that the effectiveness decreases with the increase in the volume flow rate of nanofluid. The effectiveness decreases due to the decrease in outlet temperature of nanofluid as the volume flow rate increases. Similar trends of effectiveness are reported in some previous studies [59, 60]. However, with the concentration of nanoparticles, the effectiveness increases for each nanofluid. This is due to the higher outlet temperatures with increasing particle concentration.

As depicted in Fig. 10 (Sect. 4.2), the exergy loss reduces as the concentration of nanoparticles increases for each nanofluid. The lowest exergy loss is found for CuO nanofluids, while these losses have maximum value in the case of TiO$_2$ nanofluids.
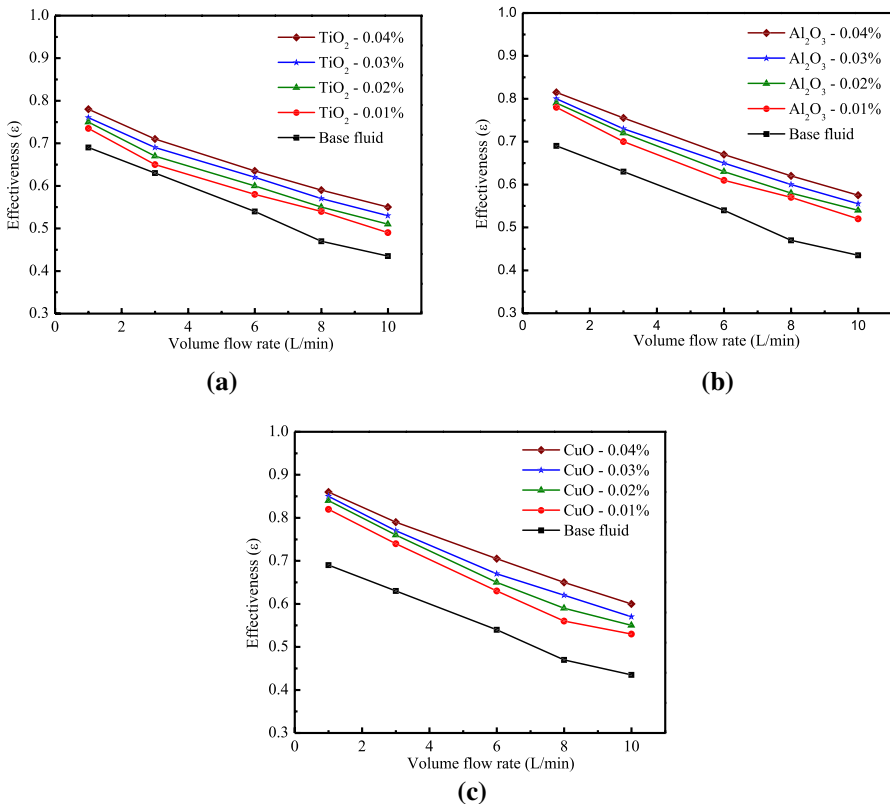

Fig. 16 Variation in effectiveness with the volume flow rate at 0.04 vol.% of particle concentration for (a) TiO$_2$ nanofluids, (b) Al$_2$O$_3$ nanofluids, and (c) CuO nanofluids

If the effectiveness is compared with the exergy losses for the same volume flow rate, it is concluded from Figs. 10 and 16 that for a lower value of exergy loss the effectiveness is found higher and vice versa. Similar trends of effectiveness and exergy losses were also reported by Gerken et al. [61]. For the present study, the average enhancement in the effectiveness is found 30.38%, 24.23%, and 18% for CuO, Al_2O_3, and TiO_2 nanofluids, respectively, at 0.04 vol. %. It is clear from the present study that increasing the nanoparticles in the base fluid increases the heat transfer rate and decreases the exergy loss (Fig. 10). Hence, the heat transfer effectiveness (Fig. 16) of the heat exchanger increases [62].

4 Conclusions

In this study, the second law characteristics of three different CMC-based non-Newtonian nanofluids through a helical coil heat exchanger are evaluated. The effect of nanoparticles, volume fraction of nanoparticles, and inlet temperature of hot fluid in helical coil heat exchanger are studied. The significant findings of the present study are as below:

1. For the authenticity of experimental results, validation for Nusselt number and friction factor has been performed with different correlation and numerical results. The experimental Nusselt numbers are in the acceptable range with the theoretical correlations with a maximum variation of 13.8%. The numerical Nusselt number maximum deviated by 13.9% with experimental values, while the experimental friction factor maximum deviated by 10.7% and 18.33% with the theoretical correlation and numerical results, respectively.
2. On increasing particle concentration from 0.01% to 0.04 vol.%, the total exergy loss reduced by 14%, 30%, and 33% for TiO_2, Al_2O_3, and CuO nanofluids, respectively, as compared to the base fluid.
3. The maximum second law efficiency for base fluid has been found to be 67%. It is observed that on increasing the particle volume fraction from 0.01% to 0.04% the second law efficiency can be improved to 71%, 74%, and 77% for TiO_2, Al_2O_3, and CuO non-Newtonian nanofluids, respectively.
4. The exergy loss and second law efficiency are compared for experimental and numerical study. It is concluded that the numerical exergy loss is deviated from the experimental values by 15.5%, 15%, and 16% for Al_2O_3, CuO, and TiO_2 nanofluids, respectively, while the maximum deviation in second law efficiency is 13%, 14.5%, and 17% for Al_2O_3, CuO, and TiO_2 nanofluids, respectively.
5. It is also observed that the exergy loss increases as the inlet temperature of hot fluid increases, due to the higher temperature differences between the hot fluid and cold nanofluid.
6. The effectiveness is increasing with the particle concentration of nanofluids. If effectiveness is compared with exergy loss, for a lower value of exergy loss, the effectiveness is found higher and vice versa.

References

1. T. Alam, M.H. Kim, A comprehensive review on single phase heat transfer enhancement techniques in heat exchanger applications. Renew. Sustain. Energy Rev. **81**, 813–839 (2018)
2. B. Sundén, J. Fu, *Aerospace Heat Exchangers: Heat Transfer in Aerospace Applications* (Academic Press, Oxford, 2017), p. 89
3. R. Sheikh, S. Gholampour, H. Fallahsohi, M. Goodarzi, M. Mohammad Taheri, M. Bagheri, Improving the efficiency of an exhaust thermoelectric generator based on changes in the baffle distribution of the heat exchanger. J. Therm. Anal. Calorim. **143**, 523–533 (2021)
4. M.M. Sarafraz, M.R. Safaei, M. Goodarzi, B. Yang, M. Arjomandi, Heat transfer analysis of Ga-In-Sn in a compact heat exchanger equipped with straight micro-passages. Int. J. Heat Mass Transf. **139**, 675–684 (2019)
5. Z. Tian, A. Abdollahi, M. Shariati, A. Amindoust, H. Arasteh, A. Karimipour, … Q.V. Bach, Turbulent flows in a spiral double-pipe heat exchanger: optimal performance conditions using an enhanced genetic algorithm. Int. J. Numer. Meth. Heat Fluid Flow **30**, 39–53 (2019)
6. A.M. Hassaan, H.M. Mostafa, Experimental study for convection heat transfer from helical coils with the same outer surface area and different coil geometry. J. Thermal. Sci. Eng. Appl. **13**, 1–17 (2021)
7. S. U. Choi and J. A. Eastman, Enhancing thermal conductivity of fluids with nanoparticles (No. ANL/MSD/CP--84938; CONF-951135--29). Argonne National Lab. 1995.
8. S. Anitha, M.R. Safaei, S. Rajeswari, M. Pichumani, Thermal and energy management prospects of γ-AlOOH hybrid nanofluids for the application of sustainable heat exchanger systems. J. Thermal. Anal. Calorim. **42**, 1–17 (2021)
9. M.H. Bahmani, O.A. Akbari, M. Zarringhalam, G.A.S. Shabani, M. Goodarzi, Forced convection in a double tube heat exchanger using nanofluids with constant and variable thermophysical properties. Int. J. Numer. Meth. Heat Fluid Flow **30**, 3247–3265 (2019)
10. M.A. Alazwari, M.R. Safaei, Combination effect of baffle arrangement and hybrid nanofluid on thermal performance of a shell and tube heat exchanger using 3-D homogeneous mixture model. Mathematics **9**, 881 (2021)
11. M.M. Sarafraz, M.R. Safaei, Z. Tian, M. Goodarzi, E.P. Bandarra Filho, M. Arjomandi, Thermal assessment of nano-particulate graphene-water/ethylene glycol (WEG 60: 40) nano-suspension in a compact heat exchanger. Energies **12**, 1929 (2019)
12. S. Eiamsa-ard, K. Kiatkittipong, Thermohydraulics of TiO_2/water nanofluid in a round tube with twisted tape inserts. Int. J. Thermophys. **40**, 28 (2019)
13. M. Goodarzi, A.S. Kherbeet, M. Afrand, E. Sadeghinezhad, M. Mehrali, P. Zahedi, … M. Dahari, Investigation of heat transfer performance and friction factor of a counter-flow double-pipe heat exchanger using nitrogen-doped, graphene-based nanofluids. Int. Commun. Heat Mass Transfer **76**, 16–23 (2016)
14. M. Goodarzi, A. Amiri, M.S. Goodarzi, M.R. Safaei, A. Karimipour, E.M. Languri, M. Dahari, Investigation of heat transfer and pressure drop of a counter flow corrugated plate heat exchanger using MWCNT based nanofluids. Int. Commun. Heat Mass Transfer **66**, 172–179 (2015)
15. Z.X. Li, U. Khaled, A.A. Al-Rashed, M. Goodarzi, M.M. Sarafraz, R. Meer, Heat transfer evaluation of a micro heat exchanger cooling with spherical carbon-acetone nanofluid. Int J Heat Mass Transf **149**, 119124 (2020)
16. M. Bahiraei, H.K. Salmi, M.R. Safaei, Effect of employing a new biological nanofluid containing functionalized graphene nanoplatelets on thermal and hydraulic characteristics of a spiral heat exchanger. Energy Convers. Manage. **180**, 72–82 (2019)
17. S.M. Hosseini, M.R. Safaei, P. Estellé, S.H. Jafarnia, Heat transfer of water-based carbon nanotube nanofluids in the shell and tube cooling heat exchangers of the gasoline product of the residue fluid catalytic cracking unit. J. Therm. Anal. Calorim. **140**, 351–362 (2020)
18. G. Wang, S. Wang, J. Lin, Z. Chen, Exergic analysis of an ISCC system for power generation and refrigeration. Int. J. Thermophys. **42**, 1–23 (2021)
19. M. Bahiraei, N. Mazaheri, H. Moayedi, Entropy generation and exergy destruction for flow of a biologically functionalized graphene nanoplatelets nanofluid within tube enhanced with a novel rotary coaxial cross double-twisted tape. Int. Commun. Heat Mass Transf. **113**, 104546 (2020)
20. I. Dincer, M.A. Rosen, *Exergy: Energy, Environment and Sustainable Development* (Newnes, 2012)

21. A.R. Gorjaei, R. Rahmani, Numerical simulation of nanofluid flow in a channel using eulerian-eulerian two-phase model. Int. J. Thermophys. **42**, 1–16 (2021)

22. T.D. Manh, M. Marashi, A.M. Mofrad, A.H. Taleghani, H. Babazadeh, The influence of turbulator on heat transfer and exergy drop of nanofluid in heat exchangers. J. Therm. Anal. Calorim. **145**, 201–209 (2021)

23. B. Ranjbar, M. Rahimi, F. Mohammadi, Exergy analysis and economical study on using twisted tape inserts in CGS gas heaters. Int. J. Thermophys. **42**, 1–19 (2021)

24. M.R. Esfahani, E.M. Languri, Exergy analysis of a shell-and-tube heat exchanger using graphene oxide nanofluids. Exp. Thermal Fluid Sci. **83**, 100–106 (2017)

25. A. Jafarzad, M.M. Heyhat, Thermal and exergy analysis of air-nanofluid bubbly flow in a double-pipe heat exchanger. Powder Technol. **372**, 563–577 (2020)

26. J. Wang, S.S. Hashemi, S. Alahgholi, M. Mehri, M. Safarzadeh, A. Alimoradi, Analysis of Exergy and energy in shell and helically coiled finned tube heat exchangers and design optimization. Int. J. Refrig **94**, 11–23 (2018)

27. F. Nasirzadehroshenin, H. Maddah, H. Sakhaeinia, Investigation of exergy of double-pipe heat exchanger using synthesized hybrid nanofluid developed by modeling. Int. J. Thermophys. **40**, 87 (2019)

28. M. Miansari, M.A. Valipour, H. Arasteh et al., Energy and exergy analysis and optimization of helically grooved shell and tube heat exchangers by using Taguchi experimental design. J. Therm. Anal. Calorim. **139**, 3151–3164 (2020)

29. H. Maleki, M.R. Safaei, A.A. Alrashed, A. Kasaeian, Flow and heat transfer in non-Newtonian nanofluids over porous surfaces. J. Therm. Anal. Calorim. **135**, 1655–1666 (2019)

30. P. Zainith, N.K. Mishra, Experimental investigations on stability and viscosity of carboxymethyl cellulose (CMC)-based non-newtonian nanofluids with different nanoparticles with the combination of distilled water. Int. J. Thermophys. **42**, 1–21 (2021)

31. H.M. Ali, H. Babar, T.R. Shah, M.U. Sajid, M.A. Qasim, S. Javed, Preparation techniques of TiO2 nanofluids and challenges: a review. Appl. Sci. **8**, 587 (2018)

32. I. Wole-Osho, E.C. Okonkwo, S. Abbasoglu, D. Kavaz, Nanofluids in solar thermal collectors: review and limitations. Int. J. Thermophys. **41**, 1–74 (2020)

33. V. Trisaksri, S. Wongwises, Nucleate pool boiling heat transfer of TiO2–R141b nanofluids. Int. J. Heat Mass Transf. **52**, 1582–1588 (2009)

34. A.K. Tiwari, P. Ghosh, J. Sarkar, Particle concentration levels of various nanofluids in plate heat exchanger for best performance. Int. J. Heat Mass Transf. **89**, 1110–1118 (2015)

35. P. Zainith, N. Mishra, Experimental investigations on heat transfer enhancement for horizontal helical coil heat exchanger with different curvature ratios using CMC based non-Newtonian nanofluids. Heat Transf. Res. (2021). https://doi.org/10.1615/HeatTransRes.2021038864

36. A.M. Fsadni, J.P. Whitty, A review on the two-phase heat transfer characteristics in helically coiled tube heat exchangers. Int. J. Heat Mass Transf. **95**, 551–565 (2016)

37. Y. Lin, L. Zheng, X. Zhang, L. Ma, G. Chen, MHD pseudo-plastic nanofluid unsteady flow and heat transfer in a finite thin film over stretching surface with internal heat generation. Int. J. Heat Mass Transf. **84**, 903–911 (2015)

38. M. Bahiraei, R. Khosravi, S. Heshmatian, Assessment and optimization of hydrothermal characteristics for a non-Newtonian nanofluid flow within miniaturized concentric-tube heat exchanger considering designer's viewpoint. Appl. Therm. Eng. **123**, 266–276 (2017)

39. N. Asokan, P. Gunnasegaran, V.V. Wanatasanappan, Experimental investigation on the thermal performance of compact heat exchanger and the rheological properties of low concentration mono and hybrid nanofluids containing Al_2O_3 and CuO nanoparticles. Thermal Sci. Eng. Progress **20**, 100727 (2020)

40. M. Aleem, M.I. Asjad, A. Shaheen, I. Khan, MHD Influence on different water based nanofluids (TiO_2, Al_2O_3, CuO) in porous medium with chemical reaction and Newtonian heating. Chaos, Solit. Fractals **130**, 109437 (2020)

41. B.C. Pak, Y.I. Cho, Hydrodynamic and heat transfer study of dispersed fluids with submicron metallic oxide particles. Exp. Heat Transf. Int. J. **11**, 151–170 (1998)

42. Y. Xuan, W. Roetzel, Conceptions for heat transfer correlation of nanofluids. Int. J. Heat Mass Transf. **43**, 3701–3707 (2000)

43. P. Barnoon, D. Toghraie, Numerical investigation of laminar flow and heat transfer of non-Newtonian nanofluid within a porous medium. Powder Technol. **325**, 78–91 (2018)

44. P. Zainith, N.K. Mishra, A comparative study on thermal-hydraulic performance of different non-Newtonian nanofluids through an elliptical annulus. J Thermal Sci. Eng. Appl. **13**, 051027 (2021)
45. T.A. Pimenta, J.B.L.M. Campos, Heat transfer coefficients from Newtonian and non-Newtonian fluids flowing in laminar regime in a helical coil. Int. J. Heat Mass Transf. **58**, 676–690 (2013)
46. A. Einstein, A new determination of molecular dimensions. Ann. Phys. **19**, 289–306 (1906)
47. E.J. Wasp, J.P. Kenny, R.L. Gandhi, *Solid-Liquid Flow Slurry Pipeline Transportation* (Gulf Publishing Co., Houston, 1979)
48. A.B. Metzner, J.C. Reed, Flow of non-newtonian fluids—correlation of the laminar, transition, and turbulent-flow regions. AIChE J. **1**, 434–440 (1955)
49. B.K. Hardik, P.K. Baburajan, S.V. Prabhu, Local heat transfer coefficient in helical coils with single phase flow. Int. J. Heat Mass Transf. **89**, 522–538 (2015)
50. H.S. Dizaji, S. Jafarmadar, S. Asaadi, Experimental exergy analysis for shell and tube heat exchanger made of corrugated shell and corrugated tube. Exp. Thermal Fluid Sci. **81**, 475–481 (2017)
51. N. Mazaheri, M. Bahiraei, H.A. Chaghakaboodi, H. Moayedi, Analyzing performance of a ribbed triple-tube heat exchanger operated with graphene nanoplatelets nanofluid based on entropy generation and exergy destruction. Int. Commun. Heat Mass Transfer **107**, 55–67 (2019)
52. A. Bejan, *Advanced Engineering Thermodynamics* (John Wiley & Sons, 2016)
53. H.D. Young, *Statistical Treatment of Experimental Data* (McGraw-Hill, New York, 1962)
54. J.D. Holman, *Experimental Methods for Engineers* (McGraw-Hill, New York, 1986)
55. M. Kahani, S.Z. Heris, S.M. Mousavi, Comparative study between metal oxide nanopowders on thermal characteristics of nanofluid flow through helical coils. Powder Technol. **246**, 82–92 (2013)
56. P. Mishra, S.N. Gupta, Momentum transfer in curved pipes. 1. Newtonian fluids. Indust Eng Chem Process Des Dev **18**, 130–137 (1979)
57. A.N. Dravid, K.A. Smith, E.W. Merrill, P.L.T. Brian, Effect of secondary fluid motion on laminar flow heat transfer in helically coiled tubes. AIChE J **17**, 1114–1122 (1971)
58. R.A. Mashelkar, G.V. Devarajan, Secondary flows of non-Newtonian fluids: Part I-Laminar boundary layer flow of a generalised non-Newtonian fluid in a coiled tube. Trans. Inst. Chem. Eng. **54**, 100–107 (1976)
59. T. Srinivas, A.V. Vinod, Heat transfer intensification in a shell and helical coil heat exchanger using water-based nanofluids. Chem. Eng. Process. **102**, 1–8 (2016)
60. M.B. Fogaça, D.T. Dias, S.L. Gómez, J.J.R. Behainne, R.D.F. Turchiello, Effectiveness of a shell and helically coiled tube heat exchanger operated with gold nanofluids at low concentration: a multi-level factorial analysis. J Thermal Sci. Eng. Appl. **13**, 021029 (2021)
61. I. Gerken, J.J. Brandner, R. Dittmeyer, Heat transfer enhancement with gas-to-gas micro heat exchangers. Appl. Therm. Eng. **93**, 1410–1416 (2016)
62. M.A. Khairul, M.A. Alim, I.M. Mahbubul, R. Saidur, A. Hepbasli, A. Hossain, Heat transfer performance and exergy analyses of a corrugated plate heat exchanger using metal oxide nanofluids. Int. Commun. Heat Mass Transfer **50**, 8–14 (2014)